



Fluorescence and third-order nonlinear optical properties of thermally stable CBPEA dye-doped PMMA/ZnO nanocomposites

Mallikarjun H. Anandalli¹ · R. F. Bhajantri¹ · Shivaraj R. Maidur² · Parutagouda Shankaragouda Patil²

Received: 22 March 2020 / Accepted: 13 May 2020 / Published online: 22 May 2020
© Springer Science+Business Media, LLC, part of Springer Nature 2020

Abstract

We report the preparation and characterizations of polymethylmethacrylate (PMMA)/zinc oxide (ZnO) doped with 1-chloro-9,10-bis (phenyl ethynyl) anthracene (CBPEA) dye nanocomposite films by solution casting technique. The nanocomposite films were characterized using UV–Visible, fluorescence emission, DSC, TGA and SEM techniques. The UV–Visible confirms an increase in the absorption wavelength from 280 to 447 nm with increase in the concentration of CBPEA dye. The microstructural and dispersion of dopants were confirmed by FE-SEM studies. TGA and DSC results displayed the thermal stability of the nanocomposite films. The fluorescence spectra show the emission maximum for 1.5 wt% dye at 522 nm shifting towards higher wavelength, and anisotropic plots studies show the faster rotational diffusion with lower value of anisotropy. Further, colour parameter such as colorimetry co-ordinates (x , y), dominate wavelength (λ_d), percentage of colour purity were calculated using 1931(CIE) diagram. The PMMA/ZnO nanocomposite films doped with CBPEA fluorescence dye show blue-green emission. The nonlinear optical (NLO) properties were studied by open and closed aperture Z-scan technique using DPSS continuous wave (CW) laser operating at 532 nm wavelength. The two-photon assisted nonlinear absorption, nonlinear refraction third-order nonlinear optical susceptibility ($\chi^{(3)}$), and all-optical switching properties were determined. The switchover property of nanocomposites from reverse saturable absorption (RSA) to saturable absorption (SA) behaviour was observed. Therefore, the obtained results suggest that the fabricated films are suitable materials for optoelectronics and nonlinear optical applications.

1 Introduction

Nowadays, the research work is much devoted in preparation of polymer nanocomposites using semiconductor nanoparticles (NPs) embedding in polymer network. Recently, polymer-based nanocomposites are class of materials, have much attention in current research, due to their good optical, nonlinear optics, thermal, mechanical and structural properties and potential application in optoelectronic devices, optical sensors, electrolytes, optical fibres [1–5]. Due to the addition of semiconductor nanoparticles (TiO₂, ZnO, CdS, CdSe, ZnS, etc.) improves the linear optical and third-order nonlinear optical, structural and thermal properties of the of the polymer matrix [6–9]. The third-order nonlinear optical

materials have emerged as a promising research field with wide applications in high speed communication networks such as optical switching, frequency converters, optical switching, wavelength manipulation, high density data storage devices, optical limiting devices and signal processing devices [10–15]. The properties of the polymer nanocomposite are depending on the type of nanoparticles or fillers present in the polymer matrix. Many inorganic materials being explored as UV absorbers, among various semiconducting materials, the ZnO NPs are suitable semiconductor with good stabilizing property within polymer matrix [16, 17].

ZnO is a wide bandgap (3.37 eV), negative n -type semiconductor material with excellent chemical stability and large exciton binding energy (60 meV). ZnO has wide application in LEDs, electrodes, solar cells and luminescence at room temperature [18, 19]. Polymethylmethacrylate (PMMA) has moderate properties such as easy handling and processing, low cost, highly flexible, good transparency and light weight. In addition to these properties, PMMA has good chemical and physical properties, hence, the PMMA

✉ R. F. Bhajantri
rfbhajantri@gmail.com; rfbhajantri@kud.ac.in

¹ Department of Physics, Karnatak University, Dharwad, Karnataka 580 003, India

² Department of Physics, K.L.E. Institute of Technology, Gokul, Hubli, Karnataka 580 030, India

has wide range of applications. The polymer nanocomposite films are prepared using various methods such as spin coating, spray coating, solution casting, printing, etc [20–22]. Fluorescent dyes are the organic molecules with complex aromatic molecular structure that absorb light and re-emit it at a longer wavelength. Fluorescent dyes are low cost materials and easily soluble in polymer matrix and have a good emissivity. The fluorescent dyes have potential applications in different fields, because of wide spectral region in the visible region, shifting towards higher wavelength region [23]. Further, the fluorescent dye-doped polymer nanocomposites have wide applications in the optoelectronic and photonics devices. Dyes are playing important role in formation of charge transfer complex during reaction of fluorescence dye as a donor or electron acceptor in synthesis. Dye has conjugated system, i.e. a structure with alternating double and single bond, absorbing light in the visible spectrum. Dye-doped polymer composite exhibits good thermal, morphological and optical properties for displaying components and optoelectronic device applications [24].

Recently, Nayak et al. have reported the dispersion of ZnS nanoparticles in PMMA and studied the optical and electrical properties for OLED applications [25]. Kulyk et al. studied linear and nonlinear optical properties of PMMA/ZnO nanocomposite films [26]. A. Singh et al. recently reported the atomic layer deposition of ZnO thin films on PMMA polymer and studied its structural, morphology and photoluminescence properties [27]. Zhang et al. successfully fabricated the transparent ZnO/PMMA nanocomposites via free radical polymerization and in situ thermal decomposition, due to the dispersion of ZnO nanocrystals and the nanocomposite films exhibit good optical and thermal properties [28]. The fluorescent dyes are playing an important role in enhanced photochemical stability of polymers. Niu et al. reported the anthracene derivative dye in poly (*N*-vinyl carbazole) for blue light emitting diodes and shows good device performance with maximum quantum efficiency and brightness more than 3000 cd/m² [29]. Hong et al. studied the dispersion of ZnO in PMMA, shows good thermal and structural properties. They have shown the grafting PMMA, reduce the aggregation of ZnO nanoparticles and this causes PMMA grafted ZnO nanocomposites, enhances the thermal stability [30]. The role of derivative of fluorescent dyes have excellent photoluminescence and electroluminescence properties, used as light emitting materials. Anthracene moieties will improve the structural properties, thermal stability, good colour purity and fluorescent emission property [31, 32].

The above-mentioned research reports have motivated us to carry out the present research work. In our previous work, we confirmed a good interaction between four different concentrations of CBPEA dye-doped into PMMA/ZnO nanocomposites from the structural properties and also observed a decreasing optical energy bandgap with increasing the dye

concentration [33]. Herein, we focus on the optical properties of PMMA/ZnO polymer nanocomposite by adding higher concentration of CBPEA dye. In this study, we report the details of linear and nonlinear optical properties, thermal and morphological properties of PMMA/ZnO nanocomposites doped with CBPEA fluorescent dye. We mainly focused on fluorescence emission properties and fluorescence polarization, nonlinear optical properties with closed and open aperture Z-scan. In addition, the LED parameters such as colour co-ordinates, dominant wavelength and colour purity were calculated using fluorescence emission spectra by CIE chromaticity diagram. The thermal stability and surface morphology have also been studied. Hence, the PMMA/ZnO nanocomposites doped with CBPEA fluorescent dye can be a prominent material for optoelectronic device applications and displaying materials.

2 Experimental section

2.1 Materials

The polymer PMMA with molecular weight 400,000 g/mol was purchased from Alfa Aesar, India. Zinc oxide (ZnO) with molecular weight of 81.37 g/mol was purchased from Himedia Laboratories Pvt. Ltd India was. The organic fluorescence dye 1-chloro-9,10-bis (phenyl ethynyl) anthracene (CBPEA) with molecular weight 412.91 g/mol was purchased from Sigma Aldrich, India.

2.2 Preparation of PMMA/ZnO/CBPEA nanocomposite film

The polymer nanocomposite films were prepared by solution casting method and the experimental procedure has been reported in our previous article [33]. PMMA/ZnO composite with dispersion of 5 wt% ZnO nanoparticles into PMMA polymer and PMMA/ZnO/CBPEA composites with different wt% of CBPEA dye doping were prepared by solution casting method using the formula:

$$M(\text{wt}\%) = \frac{m_d}{m_p + m_d} \times 100 \quad (1)$$

where m_d and m_p are the mass of dopant and polymer, respectively. The photographic images of the films under room light are given in Fig. 1.

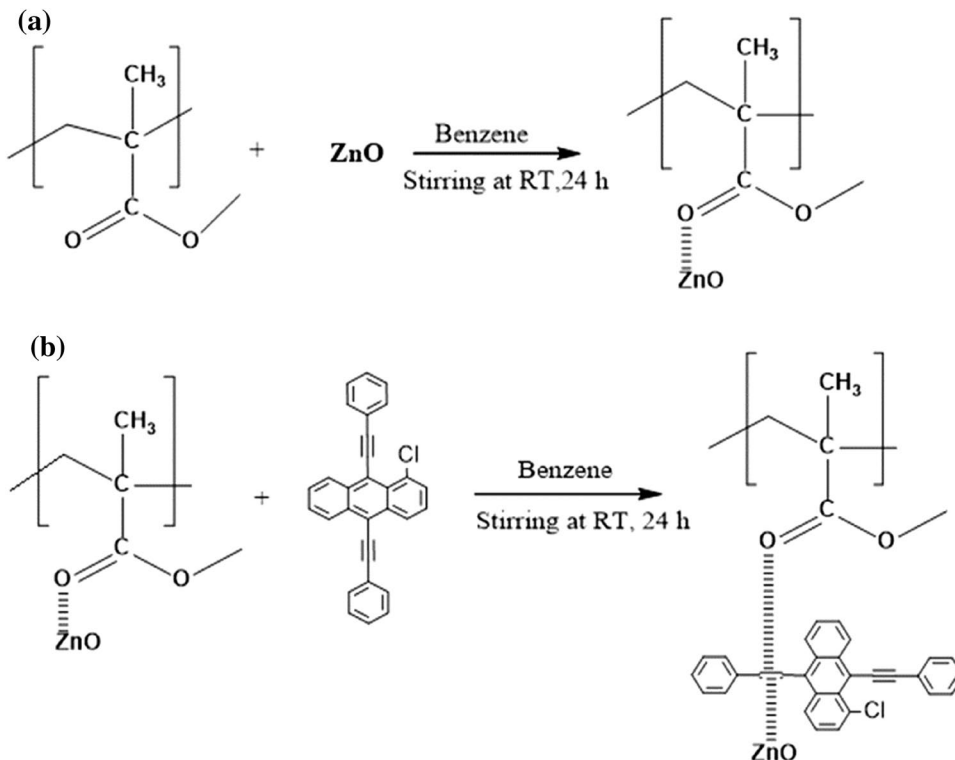
2.3 Reaction mechanism

The chemical interaction of PMMA/ZnO/CBPEA is shown in the reaction scheme given in Fig. 2a. The stepwise reaction can be explained as follows: The PMMA/ZnO

Fig. 1 Photographic images of **a** PMMA, **b** PMMA/ZnO, **c** 0.1 wt% CBPEA, **d** 0.25 wt% CBPEA nanocomposite films



Fig. 2 Reaction scheme of **a** PMMA/ZnO nanocomposite and **b** CBPEA dye-doped PMMA/ZnO polymer nanocomposite



nanocomposite solution was prepared in benzene at room temperature and stirring for 24 h. The PMMA/ZnO nanocomposite was further subjected to reaction with CBPEA in the same solvent.

The Zn nanoparticles were uniformly dispersed in PMMA matrix doped with CBPEA dye which was confirmed by SEM (Fig. 6), will be explained later. Initially, the ZnO attaches on carbonyl group of PMMA molecule and forms the electrostatic interaction. The nanocomposite upon reaction with CBPEA (containing triple bond) replace the Zn ion and forms the π -electronic interaction with oxygen atom of the carbonyl group of PMMA/ZnO nanocomposite. Further, the Zn ion present in the reaction mass finds on PMMA/CBPEA dye which is held by d -electron of Zn atom with π -bond of the dye, illustrated in reaction scheme given in Fig. 2b.

2.4 Characterization techniques

The structural, thermal, morphological properties linear and nonlinear optical properties of the selected polymer

nanocomposite films were studied using different experimental techniques. The linear absorption spectra were obtained using JASCO 750 UV–VIS–NIR spectrophotometer in the wavelength range is 200 nm to 1000 nm. The fluorescence microscopic images were recorded using ZEISS fluorescence microscope. The fluorescence emission spectra were performed using HORIBA Fluoromax fluorescence spectrometer. The thermal stability of the nanocomposite films explained using TGA STD Q600 V20.9 Build 20. The surface morphological studied using NANOSURF EZ2-FlexAFM. The CIE colour parameter was calculated using colour calculator version 7.23 software. The effect of UV light on the polymer nanocomposites films using Cole-Pormer UV Lamp 8 watt with wavelength of 365 nm and 254 nm were studied using the above-mentioned techniques.

The third-order nonlinear optical (NLO) properties of CBPEA dye-doped PMMA/ZnO polymer nanocomposites were studied using open and closed aperture Z-scan technique [34]. The main advantage of this technique is on can measure nonlinear absorption (NLA) and nonlinear refraction (NLR) simultaneously with a single scan. Open aperture

(OA) Z-scan helps to determine NLA and closed aperture (CA) Z-scan to measure NLR. In the present work, we performed Z-scan measurements with diode-pumped solid state (DPSS) continuous wave (CW) laser of Gaussian beam profile having 532 nm wavelength and 200 mW output power. Schematic of the Z-scan experimental setup is shown in Fig. 3. The laser beam was tightly focused with the plano-convex lens having 28.6 cm focal length. The beam size and the intensity of the laser at the focus point are measured to be 33 μm and 12.8 kW/cm^2 , respectively. The 1 mm cuvette containing the polymer nanocomposite solutions were placed on a stepper motor (100 μm resolution) and was scanned across the focus of the lens along the Z-axis direction (laser beam propagation). The Z-scan measurement of thin medium condition is fulfilled since the sample thickness is less than the Rayleigh length ($Z_0 = 6.15$ mm). All the power transmitted through the sample was collected in the open aperture Z-scan experiment. Whereas, only partially transmitted intensity was measured in closed aperture experiment, and the aperture size was kept at 40% of the linear transmittance ($S = 0.4$). The detectors were connected to the digital electric control unit, the translation stage and data acquisition were controlled by the computerized Z-scan program.

3 Results and discussion

3.1 UV–visible studies

The UV–Visible absorption spectra of the pure PMMA, PMMA/ZnO and CBPEA/PMMA/ZnO nanocomposite films have been measured as shown in Fig. 4. The absorption peaks of pure PMMA and PMMA/ZnO films occurs at 277 nm with very low intensity due to amorphous nature of PMMA and presence of carbonyl groups [30]. The dye-doped PMMA/ZnO nanocomposites show absorption peaks at 279 nm and increases to 285 nm assigned to $n-\pi^*$ transitions. The films with 0.1 wt%, 0.25 wt% and 0.5 wt% dye-doped PMMA/ZnO nanocomposites are showing another feeble absorption peak at 383 nm, 380 nm and 384 nm, respectively, attributed to $\pi-\pi^*$ transition of the benzene ring occurred in anthracene derivative.

The higher concentration of 0.5 wt%, 1 wt% and 1.5 wt% CBPEA dye-doped PMMA/ZnO nanocomposites shows predominant absorption peaks at 446 nm, 454 nm and 456 nm, respectively, with increasing intensity and shifting towards higher wavelengths are assigned to $\pi-\pi^*$ transition due to presence of highly conjugated carbonyl

Fig. 3 Schematic of the Z-scan experimental setup

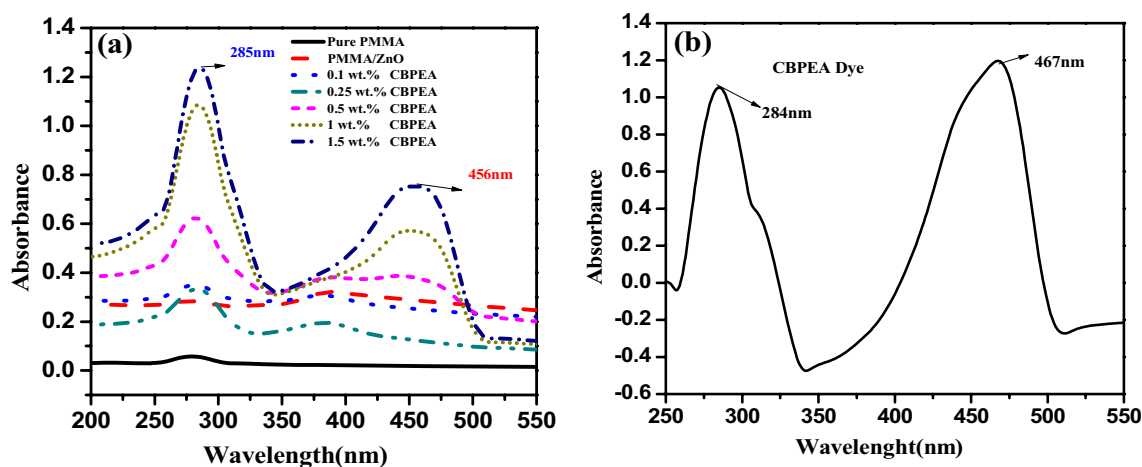
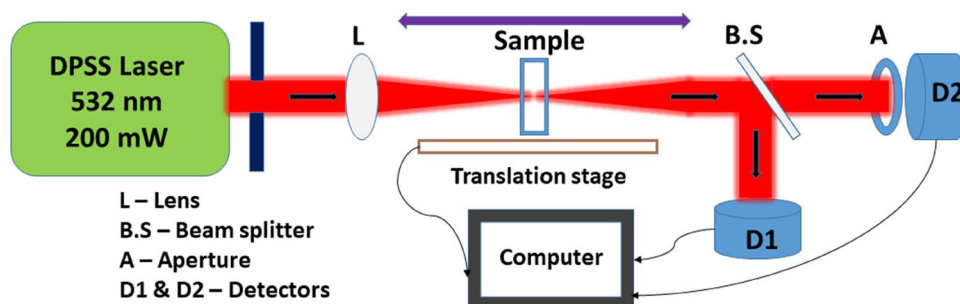


Fig. 4 UV–Vis absorption spectra of a PMMA, PMMA/ZnO and fluorescence dye-doped polymer nanocomposite and b pure CBPEA dye

functions with electron donor/acceptor complex due to intermolecular hydrogen bonding in nanocomposite [23, 35].

3.2 Thermal studies

The DSC is an effective technique to study the thermal stability of the polymer nanocomposites. Figure 5 shows the DSC thermograms of PMMA, PMMA/ZnO and CBPEA dye-doped polymer nanocomposite films. The glass transition temperature, melting temperature and degradation temperature have been determined and the results are shown in Table 1 [22, 36]. It is observed that the dispersion of ZnO nano powder in PMMA matrix will hinder the moment of macromolecules and increases the T_g . From Fig. 5, it is observed that the small changes in heat flow from exothermic to endothermic in dye-filled PMMA/ZnO composite is due to intermolecular interaction between PMMA and CBPEA dye, signifies the complete solubility of dye and dispersion of ZnO in polymer matrix [11, 17, 18]. The melting temperature (T_m) is observed around 258 °C for PMMA, shifted to 266 °C upon increase in dye concentration. The lower wt% owing to an increase in small movement of dye molecules within PMMA chain and decreases with increase in CBPEA dye. Another endothermic peak at 371 °C to 388 °C related to the degradation temperature (T_d). The degradation temperature increases with increase in concentration of fluorescence dye into PMMA/ZnO nanocomposite, due to

Table 1 DSC results of PMMA, PMMA/ZnO and PMMA/ZnO/CBPEA nanocomposites

Sample name	T_g (°C)	T_m (°C)	T_d (°C)
PMMA	138	258	371
PMMA/ZnO	148	259	371
01 wt% CBPEA	127	256	375
0.25 wt% CBPEA	125	259	375
0.5 wt% CBPEA	119	262	381
1 wt% CBPEA	115	265	386
1.5 wt% CBPEA	113	266	388

the strong intermolecular interaction between CBPEA dye and PMMA/ZnO nanocomposite. The calculated values of thermal parameter for different regions are given in Table 1.

Thermogravimetric analysis (TGA) is another reliable technique to explain the thermal behaviour and investigated the percentage of weight loss with temperature. TGA thermograms of PMMA, PMMA/ZnO and CBPEA dye-doped polymer nanocomposite films are shown in Fig. 5. The thermal stability of PMMA has enhanced upon addition of ZnO and filled with CBPEA, due to strong interfacial interaction of Zn atom with dye. From the TGA graph, it is observed that the decomposition occurred in two stages. The initial degradation appeared in the range from 150 to 200 °C with weight loss of about 7–15%, may be due to presence and evaporation of O–H molecules and benzene in the sample

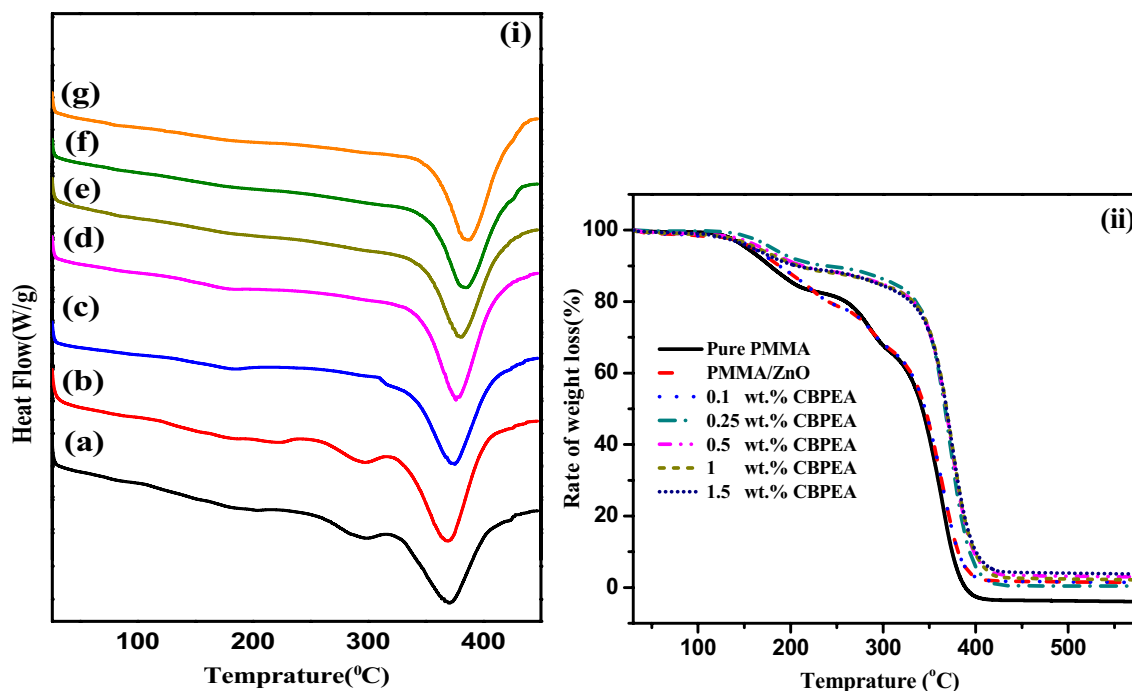


Fig. 5 i DSC and ii TGA thermograms of (a) PMMA, (b) PMMA/ZnO, (c) 0.1 wt% CBPEA, (d) 0.25 wt% CBPEA, (e) 0.5 wt% CBPEA, (f) 1 wt% CBPEA and (g) 1.5 wt% CBPEA dye-doped polymer nanocomposites

[24, 28]. The second degradation temperature appeared from 200 to 400 °C with thermal decomposition up to 350 °C is observed and the percent of weight loss decreases due to increase in dye [23, 37].

3.3 Scanning electron microscopy (SEM)

Figure 6 shows surface morphology of PMMA, PMMA/ZnO, CBPEA dye-doped PMMA/ZnO nanocomposite films recorded by field emission scanning electron microscopy (FE-SEM).

It is observed from Fig. 6, that the PMMA has a smooth surface, and 1.5 wt% CBPEA-doped ZnO/PMMA nanocomposite exhibits uniform dispersion of ZnO particles and the greater propensity to aggregate on the PMMA film, specified excellent compatibility between ZnO and PMMA [28–30]. Due to CBPEA dye doping into PMMA/ZnO nanocomposite, the surface of the polymer nanocomposite films shows tiny rods. The doping of CBPEA dye at 0.5 wt% and 1.5 wt% ascribed to possess smooth surface, compared to PMMA/ZnO [38, 39].

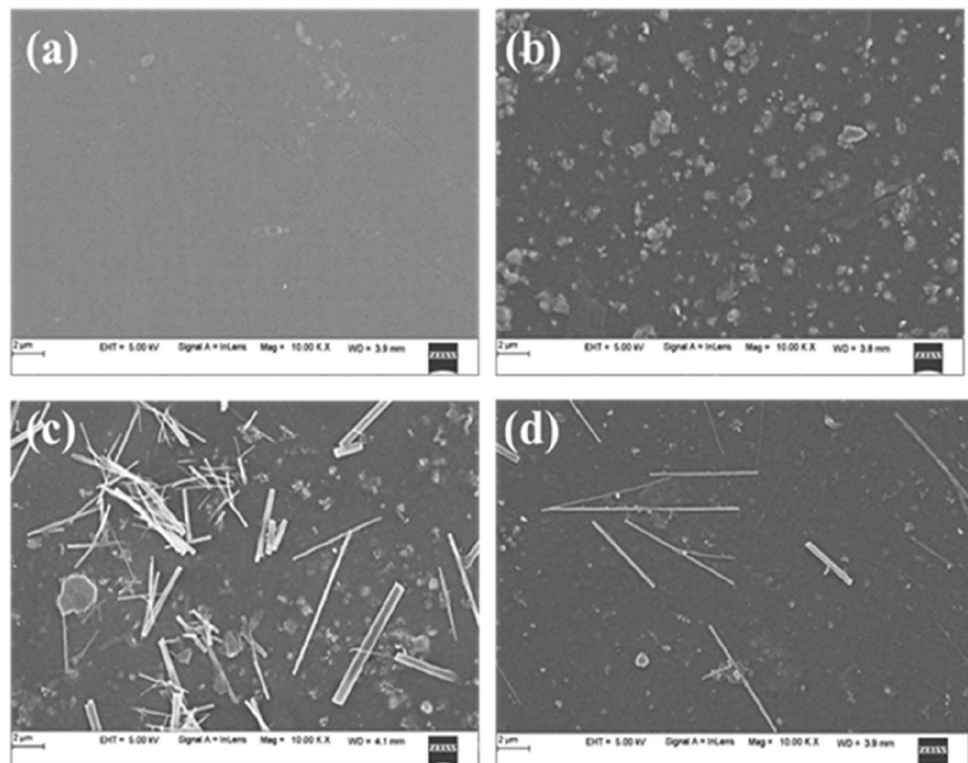
3.4 Fluorescence studies

3.4.1 Fluorescence emission

The fluorescence emission study is one of the important techniques for the optical properties of the polymer

nanocomposites. Figure 7 shows the fluorescence emission spectra of pure PMMA, PMMA/ZnO and different wt% of CBPEA dye-doped polymer nanocomposites. It was observed from the figure that the fluorescence emission occurred in the visible region and the emission wavelength was shifted towards higher wavelength due to increase in the CBPEA dye concentration in the composite. The fluorescence emission peak for pure CBPEA dye shows at 606 nm. The fluorescence emission in PMMA/ZnO composite is due to uniform distribution of ZnO nanoparticles in the polymer matrix and enhances the fluorescence property of pure PMMA. The PMMA/ZnO exhibits two emission peaks at 437 nm and 460 nm in the visible region, shifted towards higher wavelength due to dispersion of 5 wt% ZnO nanoparticles into PMMA polymer. These emission peaks in the visible region are due to radiative recombination of electrons from the conduction band and holes from the valence band of the PMMA/ZnO composite. The emission peak at 437 nm is due to presence of oxygen vacancies on the surface of ZnO and emission at 460 nm, due to presence of deep interstitial oxygen inside the ZnO [28, 40]. The fluorescence emission of PMMA/ZnO/CBPEA fluorescent dye nanocomposite shows 426 nm for 0.1 wt%, whereas the emission shows a blue-green shift towards higher wavelengths with increase in intensity at 492 nm for 0.25 wt%, 495 nm for 0.5 wt%, 498 nm for 1 wt% and 502 nm for 1.5 wt%. This clearly shows the blue-green shift of fluorescence

Fig. 6 SEM images of **a** PMMA, **b** PMMA/ZnO, **c** 0.5 wt% CBPEA and **d** 1.5 wt% CBPEA fluorescence dye-doped PMMA/ZnO nanocomposite films



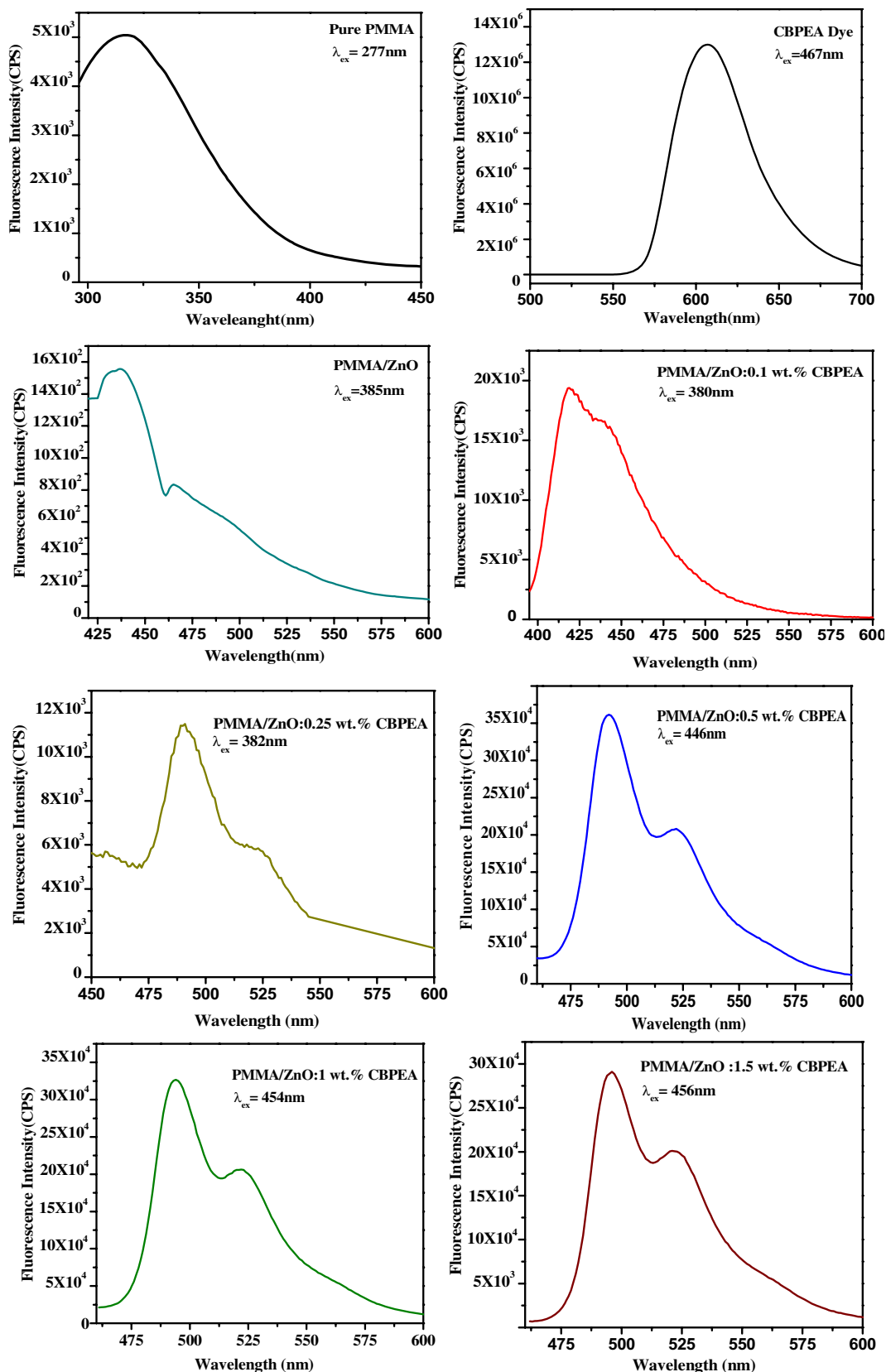


Fig. 7 Fluorescence emission spectra of PMMA, CBPEA dye, PMMA/ZnO and 0.1 wt%, 0.25 wt%, 0.5 wt%, 1 wt%, 1.5 wt% CBPEA fluorescence dye-doped PMMA/ZnO nanocomposites

emission in PMMA/ZnO/CBPEA nanocomposite is due to the possible interaction between CBPEA dye replaces the Zn ion and forms the π -electronic interaction with the oxygen atom of the carbonyl group (C=O) of PMMA/ZnO nanocomposite within the polymer matrix. The fluorophore molecules interact with the PMMA/ZnO nanocomposites, and hence might be drastically changed in the emission spectra.

Further, at higher concentration of CBPEA dye doping (0.5 wt%, 1 wt% and 1.5 wt%) in PMMA/ZnO nanocomposites, the second green fluorescence emissions were observed at 521 nm, 522 nm 525 nm. These green emissions in PMMA/ZnO/CBPEA nanocomposites can be attributed to deep level emission, caused by fluorescent dye impurities and structural defects inherent in ZnO nanoparticle such as oxygen vacancies, zinc interstitials and interaction of fluorophore containing aromatic compounds into polymer nanocomposite [1, 41]. The guest (CBPEA) molecules are probably attached to the surface of the ZnO at the oxygen vacancy sites, which significantly reduced the concentration of oxygen vacancy sites of ZnO. Thus, the fluorescence dye capping slows down the decay rate of green emission peak due to energy transfer, which supports the fact that CBPEA dye molecules are attached at the oxygen vacancy sites of the ZnO with reduced defect states [29, 42, 43].

3.4.2 Fluorescence microscopic images

Figure 8 shows fluorescence microscopic images of PMMA/ZnO and CBPEA dye-doped PMMA/ZnO nanocomposites, recorded using Zeiss fluorescence microscope exhibits green emission under blue (420 nm to 495 nm) excitation and red emission under green (510 nm to 560 nm) excitation. The same results are also observed in the lab, when the PMMA, PMMA/ZnO and CBPEA dye-doped PMMA/ZnO nanocomposite films exposed under UV light of 365 nm and the photographic images are shown in Fig. 9 [40]. The ZnO nanoparticles dispersed uniformly in polymer matrix, containing carbonyl and benzene groups in nanocomposite. Photo-induced fluorescence imaging in dye/PMMA/ZnO nanocomposites results in the strong emission, due to motion of the dye molecular segments within the polymer matrix and possibility of intermolecular interactions, such as hydrogen bonding and hydrophobic interactions from the electron-donating and electron-accepting groups. When such materials exposed to the light of different wavelengths, the fluorescence emissions occur due to photochromic reaction mechanism and such materials are called as photochromic materials, which are suitable for optoelectronic devices [37, 44].

The same results are also observed in the lab, when the PMMA, PMMA/ZnO and CBPEA dye-doped PMMA/ZnO

Fig. 8 Fluorescence microscopic images of **a** PMMA/ZnO, **b** 0.1 wt%, **c** 0.25 wt%, **d** 0.5 wt% for excitation wavelength 440 nm, **e** 1 wt% and **f** 1.5 wt% for excitation wavelength 530 nm of CBPEA dye-doped PMMA/ZnO polymer nanocomposites

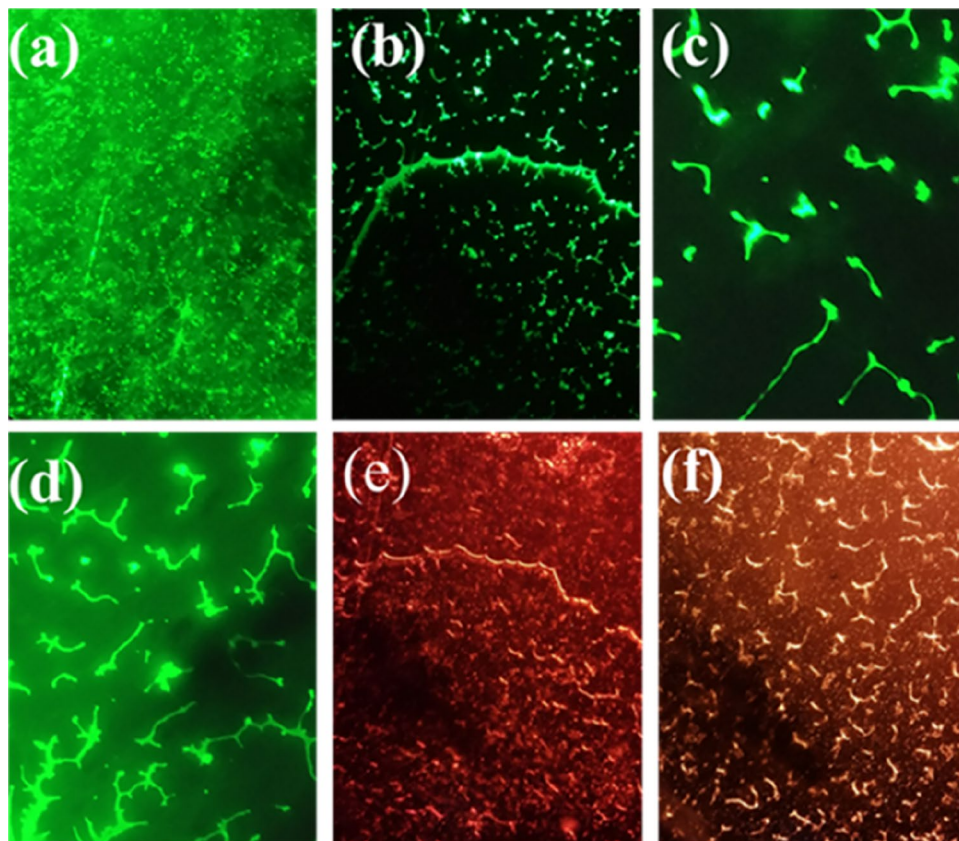




Fig. 9 Photographs of **a** PMMA, **b** PMMA/ZnO, **c** 0.1 wt% and **d** 0.25 wt% CBPEA dye-doped PMMA/ZnO polymer nanocomposite films under UV lamp of 365 nm

nanocomposite films exposed at under UV light in 365 nm the nanocomposite films emits blue-slight green emission with increasing doping material the observed photographic images are shown in Fig. 9 [40].

3.4.3 Steady state fluorescence anisotropy studies

Steady state fluorescence anisotropy is an important parameter for studying the rotational mobility of a fluorophore and molecular orientation. The anisotropy occurs, when the light emitted by the fluorophore with different fluorescence intensity along with different axes of polarization. It is working on the principle of photo-selective excitation of fluorophores with polarized light. The higher the value of fluorescence anisotropy, the faster the rotational diffusion, the lower the value of anisotropy, the slower the rotational diffusion [45]. This is caused by fluorescence depolarization due to the process of fluorescence anisotropy measurements. Fluorescence anisotropy calculations are due to the exciting fluorophore molecules with polarized light and determining the fluorescence intensity both with parallel and perpendicular to the excitation polarization. Fluorescence anisotropy (r) and polarization (P) for polymer nanocomposites can be calculated using the equations [46]:

$$r = \frac{I_{VV} - I_{VH}}{I_{VV} + 2I_{VH}} \tag{2}$$

$$p = \frac{I_{HH}I_{VV} - I_{HV}I_{VH}}{I_{HH}I_{VV} - I_{HV}I_{VH}} \tag{3}$$

where I_{VV} and I_{VH} , respectively, are vertically and horizontally polarized fluorescent light, which are produced by vertically polarized excitation light

Figure 10 shows fluorescence anisotropy with wavelength for PMMA, PMMA/ZnO nanocomposites and CBPEA dye-doped PMMA/ZnO polymer nanocomposite films. The value of fluorescence anisotropy for PMMA varies from 0.1 to 0.65 with the excitation wavelength of 250 nm and varies from 0.15 to 0.07 for 420 nm excitation. The fluorescence anisotropy for 0.5 wt% CBPEA fluorescence dye-doped PMMA/ZnO nanocomposite varies from 0.02 to 0.027, and

for 1.5 wt%, it varies from 0.009 to 0.033 for the excitation of 460 nm.

Figure 10e, f show fluorescence polarization (p) graphs. Using Eq. 3. the calculated fluorescence polarization for 0.5 wt% CBPEA dye-doped PMMA/ZnO nanocomposites varies from 0.07 to 0.11, and for 1.5 wt% CBPEA dye doping it varies from 0.014 to 0.049. The polarization decreases with increase in rotation mobility [47, 48].

3.5 CIE chromaticity plot

3.5.1 Colorimetry co-ordinates

The CIE chromaticity diagram of PMMA/ZnO and CBPEA dye-doped PMMA/ZnO polymer nanocomposite films is shown in Fig. 11 using commission international d’Elairge (CIE) in 1931, denoted as CIE 1931(x, y) colour space. The CIE chromaticity colour co-ordinates (x, y) can be calculated using emission spectra by CIE 1931 diagram, CIE introduce three primaries X, Y, Z described as linearity of colour space this can be mathematically expressed as:

$$X = k \int_0^\infty p(\lambda)\bar{x}(\lambda)d\lambda, \tag{4}$$

$$Y = k \int_0^\infty p(\lambda)\bar{y}(\lambda)d\lambda \tag{5}$$

$$Z = k \int_0^\infty p(\lambda)\bar{z}(\lambda)d\lambda \tag{6}$$

where k is constant ($k > 0$), $p(\lambda)$ is spectral distributions of a given colour and $x(\lambda), y(\lambda)$ representing the amounts of the primaries $X, Y,$ and Z required to match all monochromatic colour of wavelengths (λ) of the visible spectrum. The chromaticity co-ordinates function of the tristimulus values x, y and z in CIE colour space chromaticity co-ordinates are defined as:

$$X = \frac{x}{x + y + z} \tag{7}$$

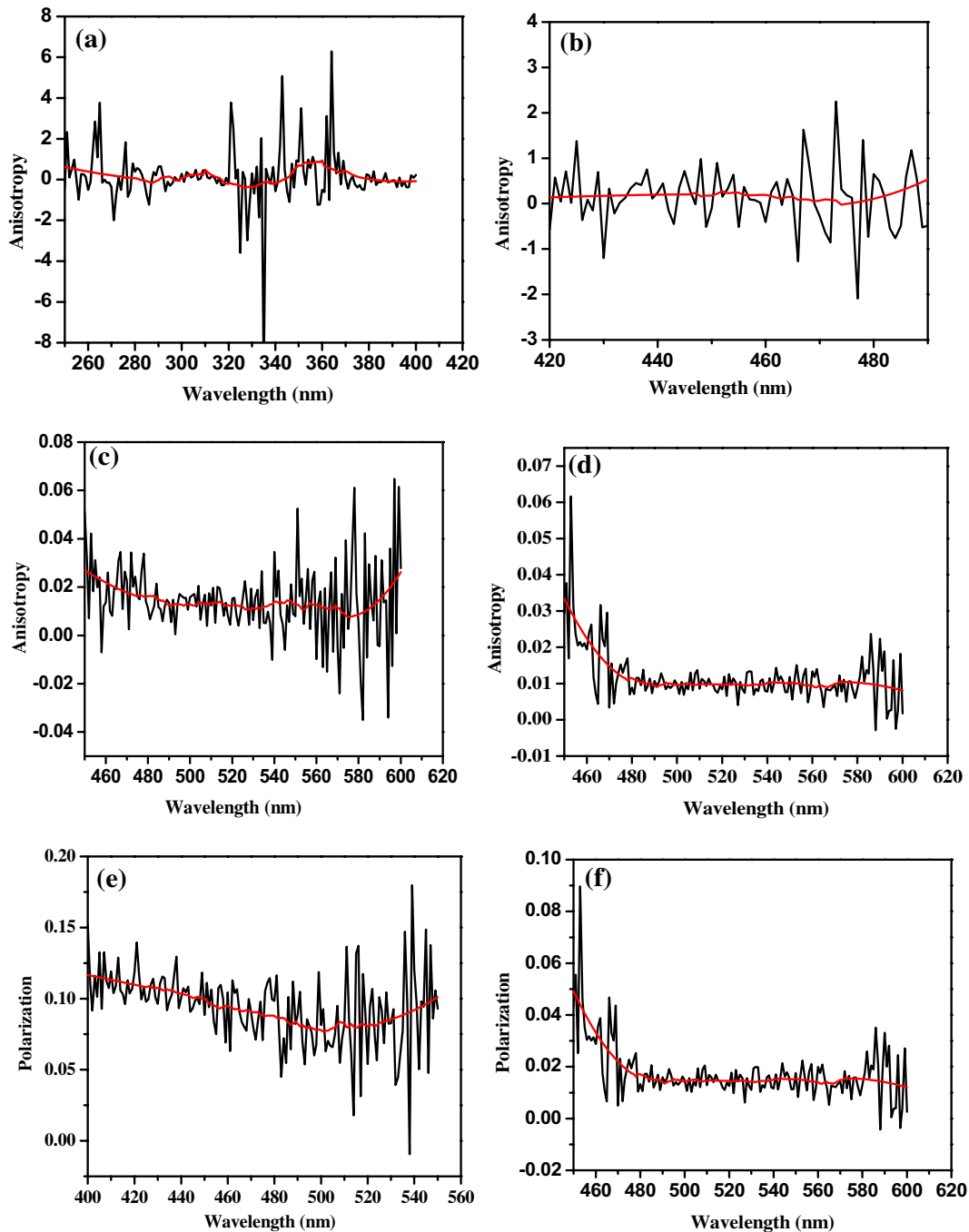


Fig. 10 Fluorescence anisotropy of **a** PMMA, **b** PMMA/ZnO, **c** 0.5 wt% CBPEA, **d** 1.5 wt% CBPEA and polarization of **e** 0.5 wt% CBPEA, **f** 1.5 wt% CBPEA dye-doped PMMA/ZnO nanocomposite

$$Y = \frac{y}{x + y + z} \quad (8)$$

$$Z = \frac{z}{x + y + z} \quad (9)$$

Equations (7), (8) and (9) colour space chromaticity co-ordinates only two chromaticity co-ordinates which are sufficient to explain the colour chromaticity. In order to calculate the dominant wavelength, we must first introduce the identification of a colour by its x , y chromaticity co-ordinates as plotted in the chromaticity diagram [49, 50]. The x , y

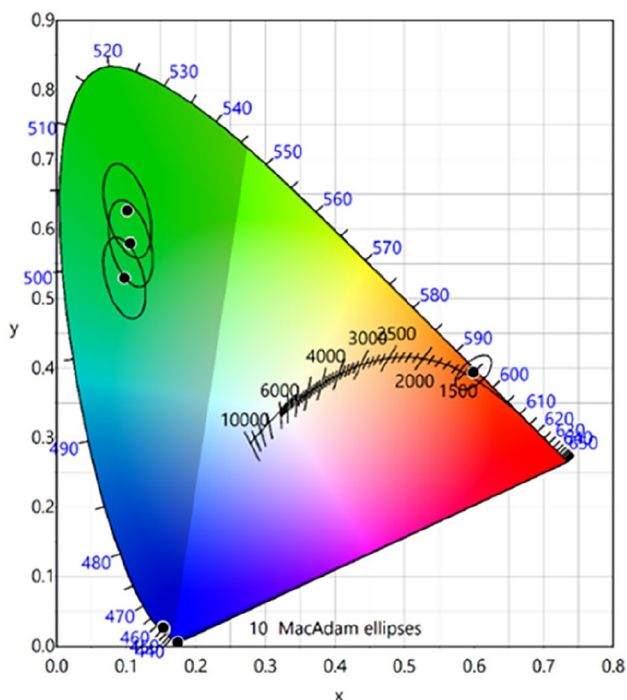


Fig. 11 CIE 1931 Chromaticity diagram of PMMA/ZnO and PMMA/ZnO/CBPEA polymer nanocomposites showing the colorimetric coordinates in the blue-green region

Table 2 Colour parameters using CIE 1931 diagram of ZnO/PMMA/CBPEA dye nanocomposite

Sample	<i>x</i>	<i>y</i>	Dominant wavelength (nm)	Colour purity (%)
CBPEA dye	0.5994	0.3935	595	98.5
PMMA	0.1744	0.0051	317	–
PMMA/ZnO	0.1529	0.0274	457	98.8
0.1 wt% CBPEA	0.1548	0.0239	454	99.0
0.25 wt% CBPEA	0.1532	0.0266	456	98.8
0.5 wt% CBPEA	0.0974	0.5292	498	86.4
1 wt% CBPEA	0.1061	0.5790	502	80.7
1.5 wt% CBPEA	0.1019	0.6261	504	83.9

Table 3 Shows the obtained values of nonlinear phase shift ($\Delta\phi$), NLA coefficient (β), NLR coefficient (n_2), susceptibility ($\chi^{(3)}$), second hyperpolarizability (γ_h) of pure PMMA and PMMA/ZnO composites under CW laser excitation at 532 nm

Sample	$\Delta\phi$	$\beta \cdot 10^{-5}$ (cm/w)	$n_2 \cdot 10^{-8}$ (cm ² /w)	Re $\chi^{(3)}$ 10^{-7} esu	Im $\chi^{(3)}$ 10^{-8} esu	$\chi^{(3)}$ 10^{-7} esu	$\gamma_h \cdot 10^{-26}$ esu	<i>W</i>	<i>T</i>
PMMA	2.10	14.8 ± 0.1	–1.53 ± 0.05	–8.14	3.34	8.14	3.87	3.68	0.52
PMMA/ZnO	3.10	2.90 ± 0.2	–2.28 ± 0.1	–12.2	0.65	12.2	5.77	4.34	0.07
0.1 wt% CBPEA	1.80	7.20 ± 0.1	–1.34 ± 0.2	–7.14	1.63	7.14	3.39	2.15	0.29
0.25 wt% CBPEA	1.35	10.2 ± 0.25	–1.08 ± 0.15	–5.74	2.30	5.75	2.73	1.86	0.50
0.5 wt% CBPEA	1.60	–26.5 ± 0.3	–1.31 ± 0.1	–7.00	–5.98	7.03	3.34	1.87	1.07
1 wt% CBPEA	2.50	–16.5 ± 0.15	–0.36 ± 0.2	–1.93	–3.72	1.97	0.93	1.06	2.43
1.5 wt% CBPEA	2.70	–9.30 ± 0.2	–0.22 ± 0.1	–1.16	–2.10	1.18	0.56	1.07	2.28

co-ordinates of the light source can be considered to be mixture of saturated light of a specific dominant wavelength and white light, called an illuminate, explained using CIE.

3.5.2 Dominant wavelength (λ_d)

In the present study, the (*x*, *y*) colour co-ordinates visible on the edge of the colour space of the prepared polymer nanocomposites [49]. The dominant wavelength of PMMA/ZnO and dye-doped PMMA/ZnO nanocomposites was calculated with the help of calorimetric co-ordinates, which is belonging to blue-green emission and given in Table 2.

3.5.3 Colour purity

The measurement of colour purity is an important characteristic of the light emitting devices. Colour purity is the weighted average of the (*x*, *y*) co-ordinates relative to the co-ordinates of the illuminate and the co-ordinates of the dominant wavelength.

$$\text{Colourpurity} = \frac{\sqrt{(x - x_i)^2 + (y - y_i)^2}}{\sqrt{(x_d - x_i)^2 + (y_d - y_i)^2}} \times 100\% \quad (10)$$

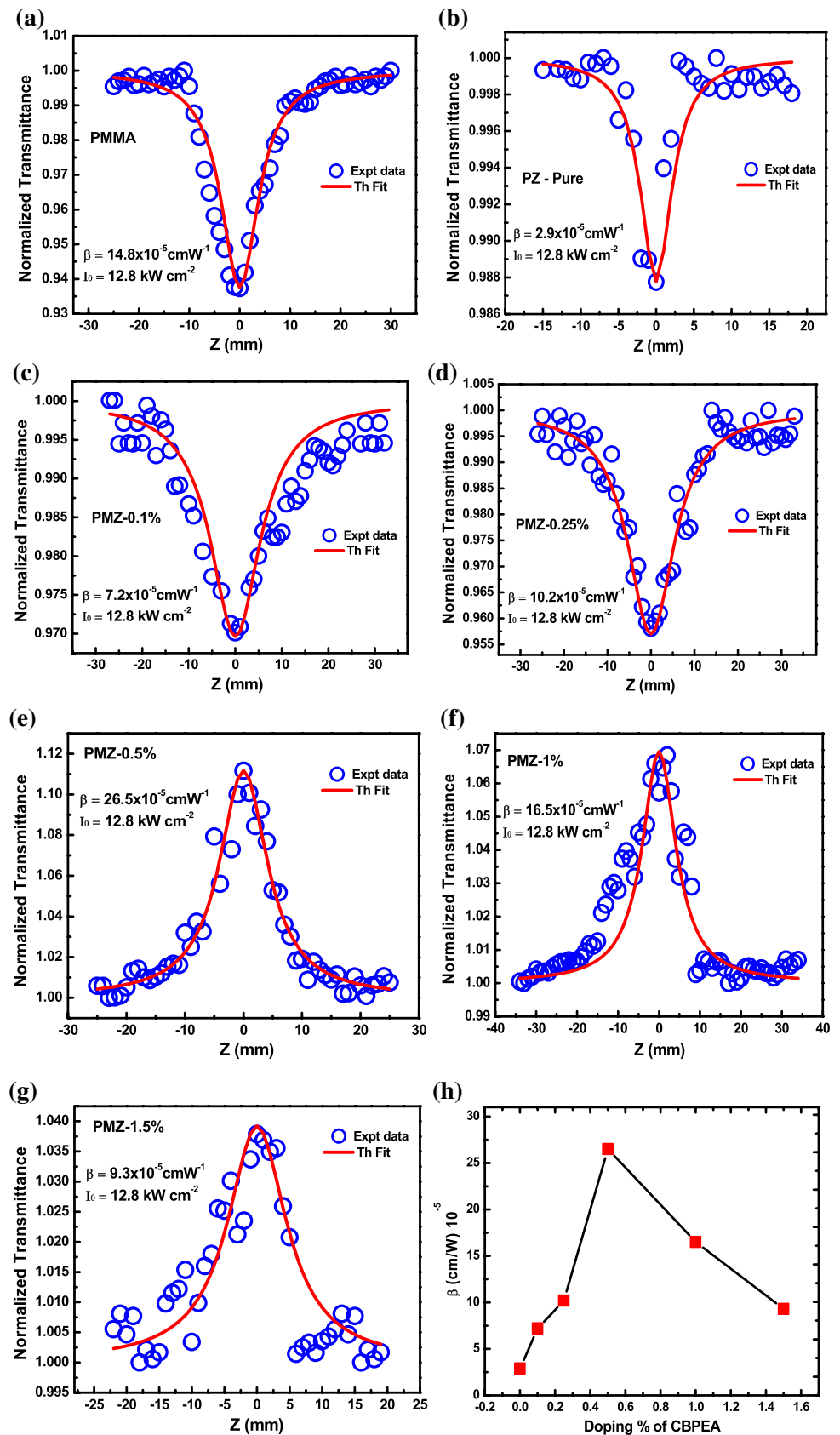
The pure CBPEA fluorescence dye shows 98.5% colour purity and ZnO/PMMA nanocomposite films show 98.8% colour purity as shown in Table 3 and the prepared films exhibit blue colour [50]. The maximum colour purity of 99% observed for 0.1 wt% of CBPEA dye-doped ZnO/PMMA nanocomposite film.

3.6 Nonlinear optical studies

3.6.1 Nonlinear absorption

The open aperture z-scan curves of the PMMA/ZnO/CBPEA polymer nanocomposites are shown in Fig. 12. It is observed that pure PMMA and PMZ composites show two different nature of nonlinear absorptions. Pure

Fig. 12 Nonlinear absorption curves of **a** pure PMMA, **b** PMMA/ZnO **c** CBPEA – 0.1 wt% **d** CBPEA – 0.25 wt% **e** CBPEA – 0.5 wt% **f** CBPEA – 1 wt% **g** CBPEA – 1.5 wt% and **h** doping effect of CBPEA dye on nonlinear absorption of PMMA/ZnO nanocomposites



PMMA, PMMA/ZnO, CBPEA – 0.1 wt% and CBPEA – 0.25 wt% show the reverse saturable absorption (RSA) behaviour, i.e. the absorption is maximum at the focus where the intensity is maximum ($Z=0$). Whereas, CBPEA – 0.5 wt%, CBPEA – 1 wt% and CBPEA – 1.5 wt% composite show the saturable absorption (SA) behaviour, i.e. the transmitted intensity of the sample reaches maximum at the focus point ($Z=0$). Therefore, sign of the nonlinear absorption is positive for SA ($\beta < 0$) and positive for RSA ($\beta > 0$). The switchover property from reverse saturable to saturable absorption (RSA to SA) has been observed for PMMA/ZnO/CBPEA nanocomposites at 0.5 wt% doping of CBPEA dye. In case of saturable absorbers, the molecules in the ground state become excited into the higher energy state at sufficiently high intensity (saturation intensity). When there is insufficient time for the molecules to decay back to the ground state before the ground state becomes depleted, the absorption subsequently saturates. These type of SA behaviour is usually observed in various dye molecules, and they are useful in laser cavities for passive Q-switching and mode-locking applications in the production of ultrafast laser pulses [51].

In order to estimate the nonlinear absorption coefficients quantitatively and to confirm the corresponding nonlinear absorption (NLA) mechanism, we fitted the experimental open aperture data with the theoretical NLA model. The solid lines in Fig. 12 represents the theoretical curves, and open circles are experimental data. The two-photon absorption type nonlinear absorption was found to be the best approximation since the energy bandgap of selected polymer nanocomposites are corresponding with the energy of two photons ($E_g \sim 2h\nu$). The normalized transmission as a function of sample position is given by,

$$T(Z) = 1 \pm \frac{\beta I_0 L_{\text{eff}}}{2\sqrt{2}(1 + Z^2/Z_0^2)} \quad (11)$$

where, β is the two-photon absorption coefficient, which is found to be in the order $\sim 10^{-5} \text{ cmW}^{-1}$ for all the samples. $L_{\text{eff}} = (1 - \exp^{-\alpha L})/\alpha$ is the effective length of the sample, α is the linear absorption coefficient and L is thickness of the sample. I_0 is the intensity of the laser beam at the focus. The corresponding β values of the samples are presented in Table 3.

3.6.2 Nonlinear refraction (NLR)

The nonlinear refraction curves of the PMMA/ZnO/CBPEA polymer nanocomposites are shown in Fig. 13. We observed negative nonlinear refraction behaviour for all the samples. The nonlinear phase shift of the samples obtained by fitting the closed aperture data with the following relation:

$$T(Z) = 1 - \frac{(4X\Delta\phi_0)}{(X^2 + 1)(X^2 + 9)} \quad (12)$$

where, $T(Z)$ is the normalized transmittance, $\Delta\phi_0$ is the nonlinear phase shift, and $X=Z/Z_0$. Nonlinear refractive index n_2 can be calculated using the $\Delta\phi_0$ value in the relation $\Delta\phi_0 = kn_2 I_0 L_{\text{eff}}$, where $k (= 2\pi/\lambda)$ is the wave vector. The obtained values of the NLR coefficients are found to be in the order $\sim 10^{-8} \text{ cm}^2 \text{ W}^{-1}$ and are given in Table 3.

The third-order nonlinear refraction and absorptions are directly related to the real and imaginary part of the third-order nonlinear optical susceptibility, respectively. The real, imaginary and magnitude of the susceptibility of the PMMA/ZnO/CBPEA polymer nanocomposites were determined using the following relations [52]:

$$\chi^{(3)} = \chi_R^{(3)} + i\chi_I^{(3)} \quad (13)$$

$$\chi_R^{(3)}(\text{esu}) = \frac{cn_0^2}{120\pi^2} n_2 \left(\frac{m^2}{W} \right) \quad (14)$$

$$\chi_I^{(3)}(\text{esu}) = \frac{c^2 n_0^2}{240\pi^2 \omega} \beta \left(\frac{m}{W} \right) \quad (15)$$

where c is the velocity of light, n_0 is the linear refractive index and ω is the angular frequency of the incident photons. The obtained magnitude of the NLO susceptibility of pure PMMA and PMMA/ZnO/CBPEA nanocomposites are found to be in the order $\sim 10^{-7}$ esu. Further, the molecular second hyperpolarizability (microscopic polarizability) of the samples is also calculated and the values are found to be in the order $\sim 10^{-26}$ esu. The obtained NLO parameters of polymer nanocomposites are compared with that of reported materials under various continuous wave laser excitations and are given in Table 4. It is found that the obtained results for PMMA/ZnO/CBPEA nanocomposites are found to be comparable with the reported materials.

Further, the one photon (W) and two-photon (T) figures of merit for all-optical switching applications have been studied. These two figures of merit decide the materials suitability in the optical switching at the laser excitation wavelength 532 nm. The calculated figures of merit for PMZ composites have satisfied the criteria $W > 1$ and $T < 1$ up to 0.5 wt% doping percentage, and did not follow the trend thereafter. Therefore, the polymer nanocomposites could be used for all-optical switching applications only below 0.5 wt% doping. The possible reason for this behaviour may be due to the materials switchover property which is observed at 0.5 wt% doping concentration.

Fig. 13 Nonlinear refraction curves of **a** pure PMMA, **b** PMMA/ZnO, **c** CBPEA – 0.1 wt%, **d** CBPEA – 0.25 wt%, **e** CBPEA – 0.5 wt%, **f** CBPEA – 1 wt%, **g** CBPEA – 1.5 wt% and **h** doping effect of CBPEA dye on nonlinear refraction of PMMA/ZnO composites

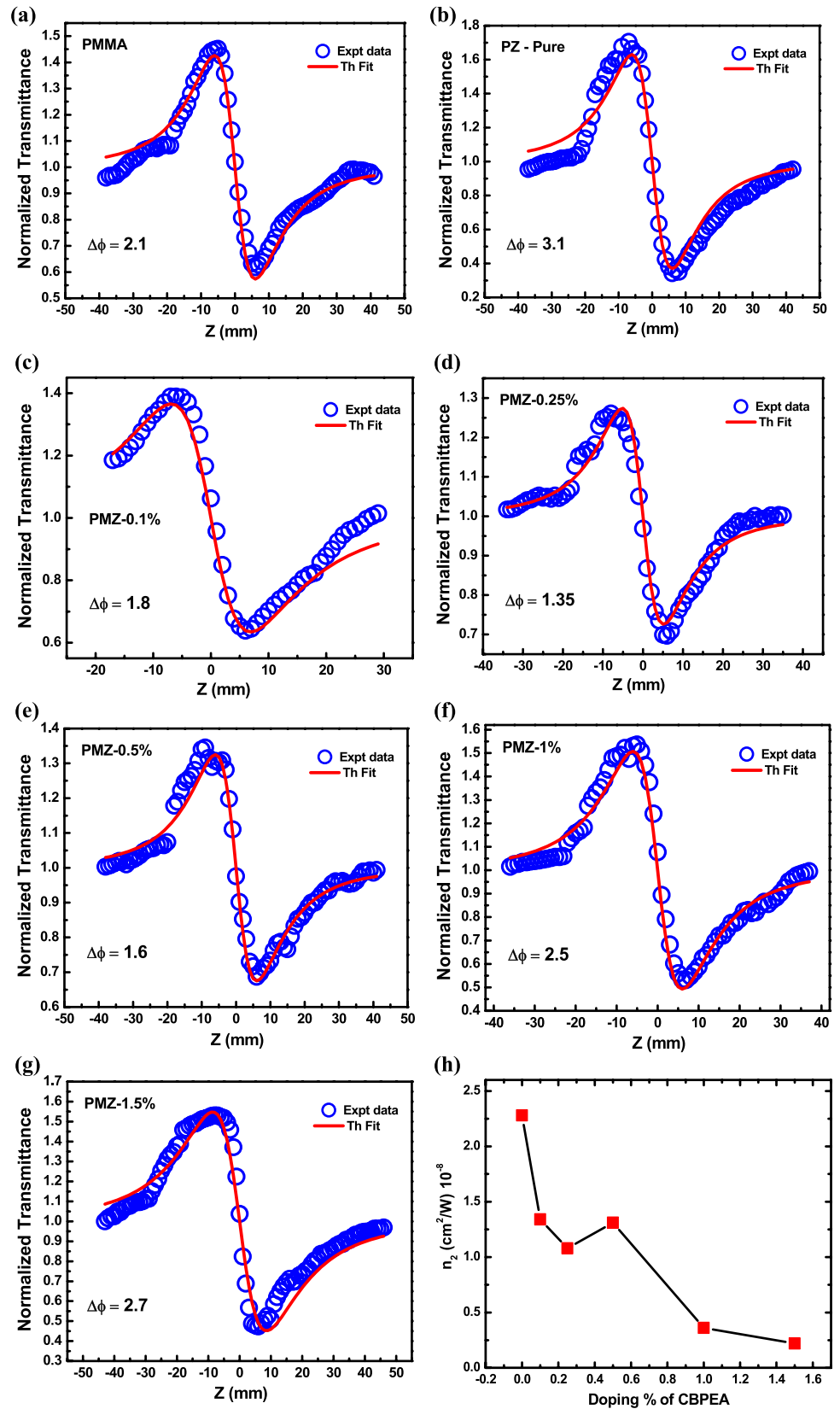


Table 4 Comparison of NLO parameters of PMMA/ZnO/CBPEA polymer nanocomposites with some of the reported materials

Material	Laser source	β 10^{-4} (cm/W)	n_2 10^{-7} (cm ² /W)	$ \chi^{(3)} $ 10^{-6} (esu)	References
Celestin blue B dye/PMMA film	532 nm; 100 mW	− 1.6	− 0.65	1.66	[53]
Leishman dye/PMMA film	532 nm; 100 mW	− 37.26	− 4.18	31.56	[54]
PR-PVA nanocomposite films	442 nm	− 380.0	−	5.91	[55]
C ₆₀ -doped PMMA	635 nm; 20 mW	3.56	− 0.93	5.64	[56]
Giemsa dye/PMMA film	532 nm; 100 mW	− 11.72	− 1.45	11.43	[57]
AB 10B dye/PVA films	633 nm; 21 mW	− 16.0	− 1.66	2.06	[58]
MNC chalcone/PMMA film	532 nm; 200 mW	1.34	−	0.049	[59]
N-ANC chalcone/PMMA film	532 nm; 200 mW	− 82.1	− 0.077	1.44	[60]
Phthalocyanine/PMMA films	633 nm; 15 mW	− 610	− 71	400	[61]
5 wt% Mn-doped ZnO films	633 nm; 22 mW	3.23×10^4	− 319	360	[62]
PMZ-0.5 wt%	532 nm; 200 mW	− 2.65	− 0.13	0.70	Present

3.6.3 Doping effect of CBPEA dye on PMZ

Figures 1h and 13h show the doping effect of CBPEA dye on nonlinear absorption (β) and nonlinear refraction (n_2) of PMMA/ZnO/CBPEA nanocomposites, respectively. It is observed from Fig. 12h that the nonlinear absorption linearly increases with the increase in doping percent of CBPEA dye up to 0.5 wt% and decreases linearly thereafter. The magnitude of nonlinear absorption of CBPEA – 0.5 wt% nanocomposites is found to be larger as compared to other composites and pure PMMA polymer. However, the nonlinear absorption behaviour switches from RSA to SA at 0.5 wt% doping concentration and retains the same characteristic behaviour for higher concentrations also. It demonstrates the switchover behaviour of composites due to the presence of CBPEA dye which is effective only above 0.5 wt% doping. Because, in order to absorb large number photons, the adequate number of dye molecules are required so that the molecular transition takes place from ground to excited state. This adequacy of molecular concentration of CBPEA dye was found at 0.5 wt% doping, as a result the switchover behaviour from RSA to SA takes place. From Fig. 13h, it is clear that the magnitude of nonlinear refraction is larger for pure PMMA/ZnO and pure PMMA which linearly decreases as the doping percent of CBPEA dye increased from 0.1 to 1.5 wt%. The change in NLO properties with respect to dye doping is due the structural and transmittance changes in the films. The large number of dye molecules conjugated with PMMA/ZnO films enhanced the absorption of more number of photons which increases nonlinear absorption (β) till 0.5 wt% and decreases thereafter due to the switchover behaviour from RSA to SA. Whereas, the nonlinear refraction (n_2) decreases with increase in dye molecules due to the structural changes of the films. The formation of tiny rods due to the presence of CBPEA dye are the reason to observe the decrease in n_2 with doping percentage. These grains could be larger for highest doping percentage (1.5 wt%) and

thereby increasing the surface roughness of the films, which in turn decreased the n_2 . Therefore, from our studies, it is observed that the NLO properties of PMMA/ZnO/CBPEA nanocomposites have greatly influenced with the doping of CBPEA dye. In fact, the doping effect at 0.5 wt% of CBPEA has made enormous changes in the NLO results. Hence, the CBPEA dye-doped PMMA/ZnO nanocomposites could be used as saturable absorber materials in the Q-switching and mode-locking applications.

4 Conclusion

In summary, the fluorescent dye-doped PMMA/ZnO nanocomposite films were prepared using solution casting method in a polar solvent benzene. Due to capping of 1-chloro,9,10-bis (phenyl ethynyl) anthracene dye, the optical and thermal properties of PMMA/ZnO nanocomposite have been enhanced. Thermal studies confirm that the prepared nanocomposite films exhibit an increase in the thermal stability compared to pristine PMMA. The XRD results confirm an increase in the degree of crystallinity, due to presence of ZnO and fluorescent dye. SEM images show that the ZnO nanoparticles and anthracene dye derivative dispersed uniformly in the polymer matrix. Prepared polymer nanocomposites exhibit good optical properties due to presence of Zn ions and fluorescence dye. UV–Visible spectra show the absorption in the visible region and exhibit good electronic transitions. The presence of charge transfer complexes and intermolecular interaction shows an optical bandgap of 3.2 eV which decreases to 2.95 eV. The fluorescence emission shows a shift in maximum wavelength (λ_{\max}) from 436 to 522 nm, which exhibits blue-green emission due to the presence of anthracene molecules and ZnO NPs. Fluorescence anisotropy values confirms the faster rotational diffusion occurs in the nanocomposite. The CIE colorimetric plot shows the true emission of blue and green colour and

maximum colour purity of 99% is observed for 0.1 wt% of dye-doped nanocomposite films. The nonlinear optical studies under 532 nm CW laser shows the switchover properties from reverse saturable absorption to saturable absorption at 0.5 wt% dye doping. The negative nonlinear refraction was observed in all the doping concentrations. The doping effect of dye indicates the increase in nonlinear absorption up to 0.5 wt% and decreases thereafter, while nonlinear refraction linearly decreased with increase in doping percentage. Further, the optical switching studies have demonstrated the materials suitability in all-optical switching devices. Therefore, the dye-doped PMMA/ZnO nanocomposites can be useful candidates for optoelectronic and saturable absorber applications.

Acknowledgements The authors are grateful to Science and Engineering Research Board (SERB), Department of Science and Technology (DST) Govt. of India, New Delhi for the research project (Grant No. SR/FTP/PS-011/2010) and (Grant No. SB/EMEQ-089/2013). The authors also thank University Grants Commission (UGC), New Delhi for SAP-CAS Phase-II (Grant No. F.530/9/CAS-II/2015(SAP-I) for providing financial assistance. The authors are thankful to USIC and SAIF, K.U. Dharwad for providing experimental facilities.

References

- R. Balen, W.V. da Costa, A.J. de Lara, J.F. Piai, E.C. Muniz, M.V. Companhia, T.U. Nakamura, S.M. Lima, L.H. da Cunha Andrade, P.R. Bittencourt, A.A. Hechenleitner, *Appl. Surf. Sci.* **385**, 257–267 (2016)
- S. Hammami, A. Barhoum, M. Bechelany, *J. Mater. Sci.* **53**, 1911–1921 (2018)
- S.B. Aziz, R.B. Marif, M.A. Brza, A.N. Hassan, H.A. Ahmad, Y.A. Faidhalla, M.F.Z. Kadir, *Results Phys.* **13**, 102220 (2019)
- R. Viswanath, H.S. Bhojya Naik, G.S. Yashavanth Kumar, P.N. Prashanth Kumar, H.N. Harish, M.C. Prabhakar, R. Praveen, *Appl. Surf. Sci.* **301**, 126–133 (2014)
- R. Kaur, S.K. Tripathi, *Opt. Mater.* **54**, 111–119 (2016)
- R.M. Abozaid, Z.Z. Lazarevic, I. Radaviv, M. Gilic, D. Sevic, M.S. RabaSovic, V. Radojevic, *Opt. Mater.* **92**, 405–410 (2019)
- R.B. Choudhary, A. Verma, *Opt. Mater.* **96**, 109310 (2019)
- H. Song, S. Lee, *Nanotechnology* **18**, 055402 (2007)
- P.K. Khanna, N. Singh, *J. Lumin.* **127**, 474–482 (2007)
- S.J. Mathews, S.C. Kumar, L. Giribabu, S.V. Rao, *Mater. Lett.* **61**, 4426–4431 (2007)
- P. Viswanath, P.V. Rambhatla, P.S. Kiran, V.S. Muthukumar, *J. Mater. Sci.* **30**, 12447–12455 (2019)
- R.J. Sengwa, S. Choudhary, P. Dhatarwa, *J. Mater. Sci.* **30**, 12275–12294 (2019)
- T.A. Taha, *Polym. Bull.* **76**, 903–918 (2019)
- Y. Pepe, A. Karatay, Y.O. Donar, S. Bilge, A. Elmali, A. Sinag, *Opt. Mater.* **101**, 109749 (2020)
- V. Viswanath, G. Subodh, C.I. Muneera, *Opt. Laser Technol.* **127**, 106168 (2020)
- M. Tamborra, M. Striccoli, R. Comparelli, M.L. Curri, A. Petrella, A. Agostiano, *Nanotechnology* **15**, S240–S244 (2004)
- M.K. Poddar, S. Sharma, V.S. Moholkar, *Polymer* **99**, 453–469 (2016)
- B. Kulyk, V. Kapustianyk, V. Tsybul'sky, O. Krupka, B. Sahraoui, J. Alloys. *Compd* **502**, 24–27 (2010)
- M. Kahouli, A. Barhoumi, A. Bouzid, A. Al-Hajry, S. Guermazi, *Superlatt. Microstruct.* **85**, 7–23 (2015)
- V.A.L. Roy, A.B. Djurisi, W.K. Chan, J. Gao, H.F. Lui, C. Surya, *Appl. Phys. Lett.* **83**, 141–143 (2003)
- M. Khan, M. Chen, C. Wei, J. Tao, N. Huang, Z. Qi, L. Li, *Appl. Phys. A* **117**, 1085–1093 (2014)
- S. Sharma, R. Vyas, S. Shrivastava, Y.K. Vijay, *Phys. B* **406**, 3230–3233 (2011)
- V. Hebbar, R.F. Bhajantri, J. Naik, S.G. Rathod, *Mater. Res. Express* **3**, 075301–075315 (2016)
- P.-I. Shih, C.Y. Chuang, C.H. Chien, E.W.G. Diau, C.F. Shu, *Adv. Funct. Mater.* **17**, 3141–3146 (2007)
- D. Nayak, R.B. Choudhary, *Opt. Mater.* **91**, 470–481 (2019)
- B. Kulyk, B. Sahraoui, O. Krupka, V. Kapustianyk, V. Radyk, E. Berdowska, S. Tkaczyk, E. Kityk, *J. Appl. Phys.* **106**, 093102 (2009)
- A. Singh, A. Mathur, D. Pal, A. Sengupta, R. Singh, S. Chattopadhyay, *Vacuum* **161**, 398–403 (2019)
- L. Zhang, F. Li, Y. Chen, X. Wang, *J. Lumin.* **131**, 1701–1706 (2011)
- Y.H. Niu, B. Chen, T.D. Kim, M.S. Liu, A.K.Y. Jen, *Appl. Phys. Lett.* **85**, 5433–5435 (2004)
- R.Y. Hong, J.Z. Qian, J.X. Cao, *Powder Technol.* **163**, 160–168 (2006)
- J. Kido, K. Hongawa, K. Okuyama, K. Nagi, *Appl. Phys. Lett.* **64**, 815–817 (1994)
- C.V. Suneesh, K.R. Gopidas, *J. Phys. Chem. C* **113**, 1606–1614 (2009)
- M. Anandalli, T.M. Kanakaraj, V. Hebbar, J. Naik, R.F. Bhajantri, *AIP Conf. Proc.* **1953**, 030189 (2018)
- M. Sheik-Bahae, A.A. Said, T.H. Wei, D.J. Hagan, E.W. Van Stryland, *IEEE J. Quantum Electr.* **26**, 760–769 (1990)
- R.F. Bhajantri, V. Ravindrachary, A. Harisha, V. Crasta, S.P. Nayak, B. Poojary, *Polymer* **47**, 3591–3598 (2006)
- T. Sheela, R.F. Bhajantri, P.M.G. Nambissan, V. Ravindrachary, B. Lobo, J. Naik, S.G. Rathod, *J. Non Cryst. Solids* **454**, 19–30 (2016)
- A. Gultek, S. Sezer, I. Ozcan, S. Koytepe, T. Seckin, *Int. J. Adv. Res.* **5**(4), 97–111 (2017)
- V.S. Gowri, M.T.P. de Amerim, N.C. Pacheo, A.P. Souto, M.F. Esteves, S.K. Sanghi, *J. Mater. Sci.* **45**, 2427–2435 (2010)
- M.M. Demir, K. Koynov, U. Akbey, C. Bubeck, I. Park, I. Lieberwirth, G. Wegner, *Macromolecules* **40**, 1089–1100 (2007)
- S. Toyota, S. Karashima, T. Iwanaga, *Bull. Chem. Soc. Jpn* **88**, 192–199 (2015)
- A.D. Malakhov, M.V. Skorobogatyi, I.A. Prokhorenko, S.V. Gontarev, D.T. Kozhich, D.A. Stetsenko, I.A. Stepanova, Z.O. Shenkarev, Y.A. Berline, V.A. Korshum, *Eur. J. Org. Chem* **6**, 1298–1307 (2004)
- T.Y. Tou, S.S. Yap, O.H. Chin, S.W. Ng, *Opt. Mater.* **29**, 963–969 (2007)
- R.F. Bhajantri, V. Ravindrachary, B. Poojary, A. Harisha, V. Crasta, *Polym. Eng. Sci.* **49**, 903–909 (2009)
- Y.C. Chen, Z. Wang, M. Yan, S.A. Prahl, *Luminescence* **21**, 7–14 (2005)
- T. Swift, L. Swanson, S. Rimmer, *RSC Adv.* **4**, 57991–57995 (2014)
- C.M. Ingersoll, C.M. Strollo, *J. Chem. Educ.* **84**, 1313–1315 (2007)
- I. Soutar, L. Swanson, T. Annable, J.C. Padget, R. Satgurunathan, *J. Colloid Interface Sci.* **303**, 202–213 (2006)
- K.N. Kumar, R. Padma, Y.C. Ratnakaram, M. Kang, *RSC Adv.* **7**, 15084–15095 (2017)
- A.K. Bedyal, D.D. Ramteke, V. Kumar, H.C. Swart, *Mater. Res. Bull.* **103**, 173–180 (2018)

50. J. Chen, C.C. Lin, J.-Y. Lien, S.L. Wang, R.K. Chiang, *J. Mater. Chem. C* **3**, 196–203 (2015)
51. G. Xing, H. Guo, X. Zhang, T.C. Sum, C.H.A. Huan, *Opt. Express* **18**, 4564–4573 (2010)
52. S.R. Maidur, J.R. Jahagirdar, P.S. Patil, T.S. Chia, C.K. Quah, *Opt. Mater.* **75**, 580–594 (2018)
53. I.A.D.H.A. Al-Saidi, R.J. Saidi, *J. Photon. Mater. Technol* **4**, 1–7 (2018)
54. I.A.-D.H. Al-Saidi, S.A.-D. Abdulkareem, *Optik* **126**, 4299–4303 (2015)
55. S. Sreedhar, N. Illyaskutty, S. Sreedhanya, R. Philip, C.I. Muneera, *J. Appl. Phys.* **119**, 193106 (2016)
56. M.D. Zidan, M.B. Alsous, A.W. Allaf, A. Allahham, A. Al-Zier, H. Rihawi, *Optik* **127**, 2566–2569 (2016)
57. I.A. Al-Saidi, S.A.D. Abdulkareem, *Optics Laser Technol.* **82**, 150–156 (2016)
58. G. Sreekumar, P.G.L. Frobel, C.I. Muneera, K. Sathiyamoorthy, C. Vijayan, M. Chandrachur, *J. Opt. A* **11**, 125204 (2009)
59. S.R. Maidur, P.S. Patil, *Opt. Mater.* **84**, 28–37 (2018)
60. S.R. Maidur, P.S. Patil, *Optik* **190**, 54–67 (2019)
61. S.J. Mathews, S. Chaitanyakumar, L. Giribabu, S. Venugopalrao, *Optics Commun.* **280**, 206–212 (2007)
62. K.K. Nagaraja, S. Pramodini, A.S. Kumar, H.S. Nagaraja, P. Poornesh, D. Kekuda, *Opt. Mater.* **35**, 431–439 (2013)

Publisher's Note Springer Nature remains neutral with regard to jurisdictional claims in published maps and institutional affiliations.